SCIENTIFIC REPORTS

OPEN

SUBJECT AREAS:
BIOLOGICAL PHYSICS
FERROMAGNETISM
CANCER
COMPUTATIONAL METHODS

Received
18 December 2014

Accepted
9 February 2015

Published
13 March 2015

Correspondence and requests for materials should be addressed to S.R. (sir503@york.ac.uk)

Unified model of hyperthermia via hysteresis heating in systems of interacting magnetic nanoparticles

S. Ruta[1], R. Chantrell[1] & O. Hovorka[2]

[1]Department of Physics, University of York, Heslington, York YO10 5DD, United Kingdom, [2]Faculty of Engineering and the Environment, University of Southampton, Highfield, Southampton, United Kingdom.

We present a general study of the frequency and magnetic field dependence of the specific heat power produced during field-driven hysteresis cycles in magnetic nanoparticles with relevance to hyperthermia applications in biomedicine. Employing a kinetic Monte-Carlo method with natural time scales allows us to go beyond the assumptions of small driving field amplitudes and negligible inter-particle interactions, which are fundamental to the applicability of the standard approach based on linear response theory. The method captures the superparamagnetic and fully hysteretic regimes and the transition between them. Our results reveal unexpected dipolar interaction-induced enhancement or suppression of the specific heat power, dependent on the intrinsic statistical properties of particles, which cannot be accounted for by the standard theory. Although the actual heating power is difficult to predict because of the effects of interactions, optimum heating is in the transition region between the superparamagnetic and fully hysteretic regimes.

Understanding the field-driven thermally activated processes in magnetic nanoparticle (MNP) systems has been at the cornerstone of developments of applications in magnetic recording and biomedicine[1–3]. Thermal fluctuations not only determine a criterion for stability of the magnetic state (e.g. information bit) but also introduce new intrinsic time scales competing with those of external driving forces. A consistent out-of-equilibrium thermodynamic theory applicable to nanoparticle systems in this regime has not yet been developed, which radically complicates the design and optimization procedures in practice. For example, quantifying the specific heating rates in systems of MNPs with statistically distributed properties, such as those envisaged for 'heat assisted' (hyperthermia) cancer treatment methodologies[4–7], remains an unsolved issue. Although the mechanisms giving rise to heating are not fully understood, it has been suggested that hysteresis may be the dominant mechanism[7–9], and it is this mechanism which is considered here.

Generally, if the characteristic time scales of thermal fluctuation modes (τ) are long, exceeding those of fast intrinsic dynamical processes and the external field period (inverse of frequency, f^{-1}), a typical observation of field-dependent magnetization $M(H)$ is the rate-independent (static) hysteresis loop. It arises in the presence of a large number of metastable states emerging from volume and anisotropy dispersions in MNPs and the effects of inter-particle interactions. So far, self-consistent mathematically tractable calculations of the specific heat power ($\mathcal{P}$) in this limit have been only based on simplified Preisach models[10]. At the opposite extreme of time scales, $\tau \ll f^{-1}$, a system of MNPs is in thermodynamic equilibrium during the experimental time window at a given field H, defining the superparamagnetic regime[11]. This requires a fundamentally different theoretical description based on the equilibrium thermodynamics, the $M(H)$ takes the form of a Langevin function without hysteresis[11], and as a result $\mathcal{P}=0$.

At the crossover between the hysteretic and superparamagnetic regimes, i.e. when $\tau \sim f^{-1}$, direct calculations of $\mathcal{P}$ become much more difficult. Dynamical linear response theory[12] has been applied to a non-interacting system of MNPs close to equilibrium[13], hereafter referred to as Rosensweig theory (RT), which gives:

$$\mathcal{P}=\pi\mu_0\chi_0 H_0^2 f\frac{2\pi f\tau}{1+(2\pi f\tau)^2} \tag{1}$$

where χ_0 is the initial zero field equilibrium susceptibility, usually determined experimentally or calculated from the Langevin function, and H_0 is the amplitude of the sinusoidal external magnetic field of frequency f. Here the τ

depends on the intrinsic fluctuation mechanisms, often taken to relate to Brownian and/or Néel relaxation[5]. In addition to RT leading to Eq.(1), several useful phenomenological[14,15] and empirical models[6,7,16] have also been developed to evaluate $\mathcal{P}$. However, in these models and also in all of the aforementioned approaches, the interaction effects have either been ignored or are hard to access on a systematic basis.

Many studies have focused on determining the optimal conditions in terms of intrinsic properties and their distribution (particle size, anisotropy value, easy axis orientation)[9,14–17], extrinsic properties (AC field amplitude, AC field frequency)[18–20] and the role of dipole interactions[4,16,21–24], and have stressed the large influence of the distribution of magnetic properties. Also, most studies have concentrated on small field amplitude and further extensions will require going beyond the RT. Martinez-Boubeta[16] and co-workers proposed a theoretical model, valid in RT regime, including inter-particle interaction for systems of chains. To study the heating rates as function of field amplitude other authors used the standard Metropolis MC method for system of identical particles[4,21]. However it is important to note that the standard MC approach suffers from the difficulty of precise time quantification of the MC step. Landi et al. used a mean field approach for the dipole interactions[22].

Full understanding of the hyperthermia heating process requires a model incorporating these key elements: 1) it must span the full range of applicability beyond the linear response regime, 2) include the effects of intergranular interactions, and 3) be fully time-quantified to allow frequency dependent studies. Although individual investigations incorporate some of these factors, a generalised model unifying all the key factors for hyperthermia is needed if hyperthermia is to be developed and optimised as a therapy. This was also noted by Tan et. at.[25], who investigated the effects of interactions using a kinetic MC approach, demonstrating strong spatial heating variations due to variations in nanoparticle concentration.

The present work incorporates the effects of inter-particle interactions within a self-consistent kinetic Monte-Carlo (kMC) modelling framework[26]. The kMC model naturally includes the time scales of intrinsic thermal fluctuations without any further need for calibration, as opposed to Time-Quantified Metropolis Monte-Carlo methods[27], and as we will show, genuinely reproduces the superparamagnetic regime, the 'metastable' and 'dynamic' hysteresis mechanisms[28], and their frequency dependent crossover. This allows for systematic validation of the standard theories, such as RT, and establishing their range of validity in practical applications where interactions cannot be ignored. Furthermore, our approach allows us to quantify the importance of metastability in the heat production in MNP assemblies and thereby gauge its significance with respect to the superparamagnetic heating anticipated according to RT and Eq. (1).

Results

Kinetic Monte-Carlo model. The kinetic Monte-Carlo (kMC) method (see the Methods section for details) systematically incorporates the complexity of realistic particle distributions, thermal fluctuations, and time varying external fields (Fig. 1). In the present work, the uni-axial anisotropy $\vec{k}_i = K_i\hat{k}_i$, particle diameter is D_i, and particle positions are randomized as illustrated in Fig. 1(c–d). The importance of interactions is controlled by adjusting the particle packing fraction ε, with $\varepsilon = 0$ implying the non-interacting case. The system energy is:

$$E = \sum_i \left(K_i V_i \left(\hat{k}_i \times \hat{m}_i \right)^2 - V_i M_s \hat{m}_i \cdot \left(\vec{H} + \vec{H}_i^{\mathrm{dip}} \right) \right) \qquad (2)$$

with V_i being the volume of a particle i, M_s the saturation magnetization, $\hat{m}_i$ the particle moment normalized to unity. The effective local field acting on particle i is given by the sum of the external applied field, H, and the interaction field, H_i^{dip}. It can be

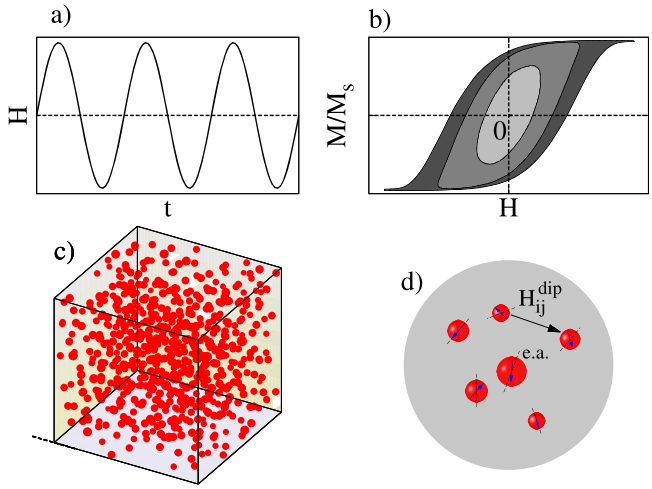

Figure 1 | Schematic illustration of key elements in the kinetic Monte-Carlo modelling framework to reproduce realistic experimental conditions. (a) Sinusoidal external driving magnetic field magnetising the particle system and producing (b) dynamical or metastable hysteresis loop depending on the applied field frequency. (c–d) Typical distribution of particles of varying positions, size, anisotropy, and controllable packing fraction allowing to tune dipolar interactions between the particles.

shown, that the formulation of the kMC approach[29] provides a direct solution method for the master-equation:

$$\frac{\partial M(t)}{\partial t} = \tau^{-1}(M_0(t) - M(t)). \qquad (3)$$

where τ is a relaxation time constant dependent non-trivially on the intrinsic relaxation times of individual particles τ_i (see the Methods section). Eq. (3) is precisely the master-equation used to originally derive Eq. (1) under the assumptions of spherical random distribution of $\hat{k}_i$ in Eq. (2) and the absence of inter-particle interactions. Hence, Eqs. (2) and (3) establish an important link between the kMC and the RT approach.

Throughout the study we consider a system of 1000 particles, and choose a parameter set typical for hyperthermia applications, specifically a sinusoidal applied field with $f = 100$ kHz and amplitude $H_0 < 600$ Oe, such that the product $H_0 f$ is below the biological discomfort level of $\approx 6 \times 10^7$ Oe/s[30]. The particle temperature is set to $T = 300$ K, thus ignoring the self-heating effect, which is equivalent to assuming infinite heat capacity of particles. We will furthermore assume variable distributions of anisotropy constant $\vec{k}_i$ and distributions of particle positions and volumes, which will allow control of the particle volumetric packing fraction ε and thus the importance of dipolar interactions. By definition, $\varepsilon = 0.0$ corresponds to a non-interacting particle system. The saturation magnetisation M_s will be initially set to 400 emu/cm^3 (i.e. magnetite like particles), and later allowed to vary to control the dipolar interaction strength further. The importance of dipolar interactions is expected to scale with the ratio of the local dipolar energy from the nearest neighbour particles to the anisotropy energy, i.e. $\zeta = M_s^2 \varepsilon / K$ (see the Methods section).

Ideal case: comparison of kMC with RT for system of identical particles. Next we use the introduced kMC model to investigate the dynamics of combined superparamagnetic and hysteretic heating mechanisms. To establish and demonstrate the link between kMC and RT it is useful to first consider a simplified system of identical particles having anisotropy axes $\hat{k}_i$ oriented parallel and along the applied field direction. To quantify the heating produced by the nanoparticles we will use the quantity called specific absorption

rate (SAR), defined as the heat dissipation $\mathcal{P}$ per unit mass (see the Methods section).

The calculated behaviour in the RT regime and beyond is shown in Fig. 2 assuming $K_i = 3 \times 10^5$ erg/cm^3 for all particles i. The solid lines in Fig. 2 show a comparison between standard calculations based on Eq.(1) and the kMC predictions. Consider first the behaviour for a maximum applied field amplitude suficiently small that the system is within the linear response regime and a direct comparison with RT is valid. For a non-interacting system both RT and kMC models predict the same optimal value of SAR. In Fig. 2(a) we show magnetization cycles starting from an initially demagnetized state. It can be seen from Fig. 2(a) that the numerical results are in good agreement with RT. The rather elliptical loops are typical of dynamic hysteresis in systems in transition from truly thermal equilibrium to fully hysteretic behaviour. Essentially, although the behaviour of the particles can be characterised as superparamagnetic from quasi-static measurements, the heating arises from the onset of dynamic hysteresis at high frequencies, which is also to be associated with superparamagnetism, as opposed to the metastable hysteresis to be discussed below.

Next we consider larger field amplitude H_0 beyond the linear response regime which is still small enough to remain within the biological discomfort limit as introduced earlier. To determine the optimal particle size for a given H_0 we have calculated SAR values as a function of mean particle diameter (D). The results are given in Fig. 2(b) for a field amplitude of $H_0 = 300$ Oe calculated using both RT and our kMC model. At this H_0 the system is in a transition region between the linear approximation and fully hysteretic behaviour, which results in pronounced deviations between the two modelling approaches. In particular, the RT considerably overestimates the peak in SAR (by $\sim 50\%$) and underestimates the corresponding optimum particle size. As a result, when using RT, the predictions for optimum particle size based on the peak in SAR are inaccurate and highly sensitive to uncertainties.

This trend is further examined in Fig. 2(c), where we systematically investigate the dependence of the optimal particle size and the maximum value of SAR on the field amplitude H_0. This is determined for every H_0 value by first finding the peak in the SAR vs. D dependence, similar to the case illustrated in Fig. 2(b). For small H_0 the system is in the linear response regime and both the peak value of SAR and the peak position as calculated from the kMC approach remain in agreement with the RT. As the H_0 increases, the RT clearly begins to underestimate the optimum particle diameter that would ideally correspond to the peak in SAR. Also, the dependence of the peak value on the field H_0 is close to quadratic (in agreement with RT) in small fields but becomes closer to linear with increasing H_0. Interestingly, decreasing the value of the uniaxial anisotropy constant, K, magnifies the non-linearity of the magnetic behaviour which, as shown in Fig. 2(d), leads to more significant variation of the peak position. As the field amplitude is limited by the biological discomfort limit, we will keep $H_0 = 300$ Oe and vary K to investigate the non-linear regime.

Non-linear regime at the crossover between superparamagnetism and metastable hysteresis in distributed particle assemblies. The above considerations based on assuming an idealised system of identical non-interacting particles clearly demonstrate that as the field amplitude H_0 increases the RT begins to significantly deviate from the equivalent benchmark kMC calculations on entering the non-linear regime. To explore the transition regime further requires including various sources of randomness as they may appear in practical applications. This includes distributions of particle diameter, D_i, and anisotropy constants, K_i, which will be assumed to take the form of realistic log-normal distributions with expectation values $D = \langle D_i \rangle$ and $K = \langle K_i \rangle$, respectively, and standard deviations set to 0.1 in both cases, and also spherically random distribution of anisotropy vectors $\hat{k}_i$.

Calculations of the dependence of SAR on D for three values of K varying in the range $0.5-3 \times 10^5$ erg/cm^3 are shown in Fig. 3. For high values of K (curve set 1 in Fig. 3), the predictions of RT reproduce the kMC calculations, since the intrinsic switching fields of

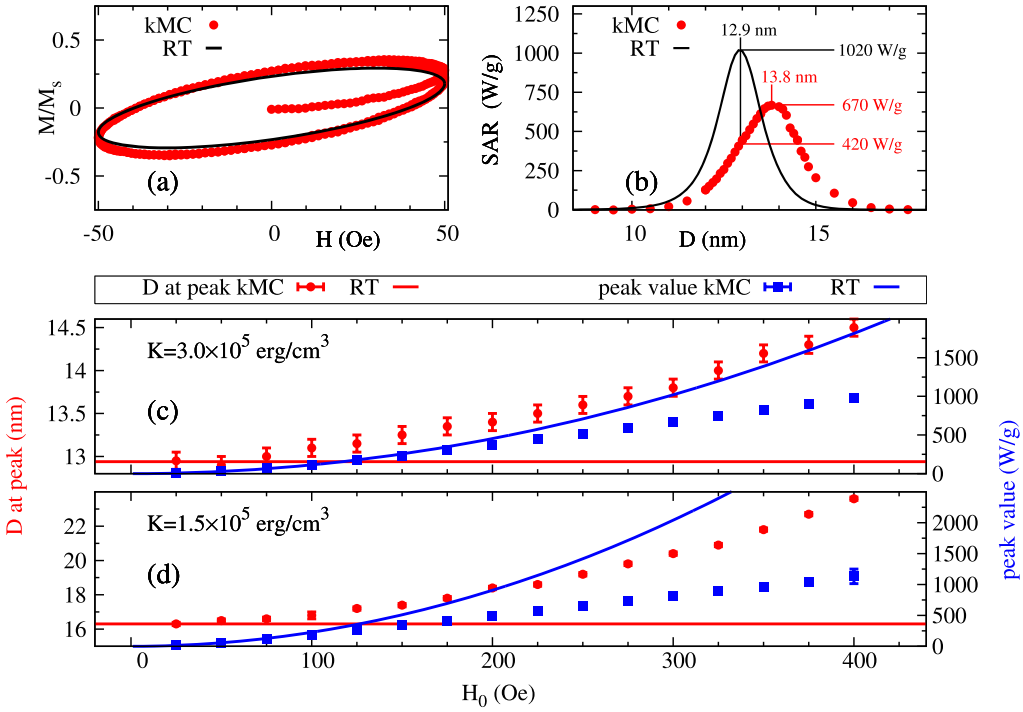

Figure 2 | Comparisons between RT (solid lines) and kMC calculation (symbols) for a system of identical particles with easy axes aligned in the field direction for: T = 300 K, M_s = 400 emu/cm^3, K = 3 × 10^5 erg/cm^3, f = 100 KHz. (a–b): Magnetisation loops for particle size of 13 nm at 50 Oe (a) and SAR as function of particle size at 300 Oe (b). (c–d): Maximum SAR value and the location of the peak in SAR for K = 3 × 10^5 erg/cm^3 (c) and K = 1.5 × 10^5 erg/cm^3 (d).

particles $H_K = 2K/M_s$ are too high in comparison to H_0, and thus the primary mechanism contributing to heating is of superparamagnetic origin leading to dynamical hysteresis loops. Increasing the particle diameter D leads to the suppression of thermal activation due to the particle moment blocking, and as a result SAR reduces to zero. On the other hand, for low values of K (curve set 3), the H_K is reduced and particle switching driven by external field through the appearance and annihilation of metastable states becomes a dominant mechanism contributing to SAR. In this regime, the RT becomes inapplicable due to the significant metastable hysteresis. Increasing D again leads to particle blocking and suppression of thermally activated behaviour, and as a result the SAR relates directly to the area of a static minor hysteresis loop limited by field amplitude H_0 which no longer depends on D, thus justifying the observed saturating trend.

The intermediate range of K (curve set 2) marks the crossover range where both mechanisms play a role, leading to a relatively broad peak for the intermediate anisotropy value. This is an important prediction since it is a major advantage from the experimental point of view, in that it reduces the need for close control of the particle mean size, while retaining a high SAR value. The overall predictions for the dependence of SAR on D begin to systematically deviate from RT as the value of K decreases, first due the nonlinearities leading to failure of the linear response theory, and thereafter due to the onset of metastable hysteresis. These observations suggest that the parameter controlling the type of behaviour is the ratio H_0/H_K. For $H_0/H_K > 1$ the behaviour is dominated by the metastable hysteresis while for $H_0/H_K \ll 1$ the SAR is of superparamagnetic origin and quantifiable by RT.

Importance of dipolar interactions. Next we investigate the effect of dipolar interactions, which have been ignored in the study so far. For this we consider a system created by the random positioning of particles in a 3D configuration, as illustrated in Fig. 1(c). Dipolar interactions are truncated and handled within the minimum image convention imposed by the periodic boundary conditions. We verified that the truncation does not affect the radial correlation function in the relevant model parameter range and thus does not modify any essential physics. We choose particle assemblies with volumetric packing fractions from the interval $\varepsilon = 0.0, \ldots, 0.14$, which gives another way of controlling dipolar effects on SAR in the particle assembly in this work besides modifying the value of M_s.

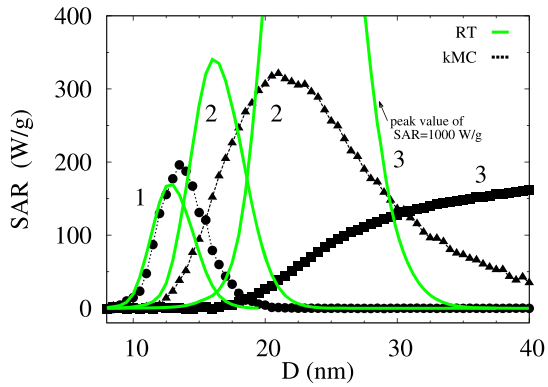

Figure 3 | Kinetic Monte-Carlo calculations of SAR as a function of the mean particle size D assuming non-interacting system, in comparison with the predictions based on the RT (solid green lines). Considered are three values of mean anisotropy constant K: 3×10^5 erg/cm^3 (circles, curve set 1 peaking at low D), 1.5×10^5 erg/cm^3 (triangles, curve set 2 peaking in the intermediate D range), and 0.5×10^5 erg/cm^3 (squares, curve set 3 saturating for large D). Calculations correspond to log-normal distributions of size and anisotropy constants both with standard deviations 0.1, spherically distributed anisotropy axes, and field amplitude $H_0 = 300$ Oe.

The dependence of SAR on the mean particle diameter for two different values of M_s is shown in Fig. 4(a). For low $M_s = 200$ emu/cm^3 the dipolar interactions are weak in comparison to the chosen anisotropy K (i.e. low $\zeta\left(=M_s^2\varepsilon/K\right)$), and as a result changing the packing fraction ε does not have any significant effect on SAR. The reduced value of M_s decreases the initial susceptibility χ_0 in Eq. (1) and thus the overall SAR. It also increases H_K, which lowers the ratio H_0/H_K leading to the suppression of the overall nonlinear behaviour and improvement of the accuracy of RT. On the other hand, for $M_s = 400$ emu/cm^3 interactions begin to play a significant role and SAR becomes dependent on ε (Fig. 4(a)). Given the assumed spherical distribution of anisotropy axes, the effect of dipolar interactions is to reduce the energy barriers separating the minimum energy states[29], and thus to lower the effective particle anisotropy in comparison to the non-interacting case value K. The χ_0 and the Néel relaxation time constant τ_N (relative to field variation time scale f^{-1}) become smaller with increasing ε, which according to Eq. (1) reduces SAR and shifts its peak towards smaller D.

In Fig. 4(b) these calculations are further extended toward the hysteretic regime by decreasing the value of K, similarly to Fig. 3, indicating that, in this regime the effect of interactions is more complex. In particular the trend can change qualitatively for small values of K, where increasing ε can even lead to enhancement of SAR (the set of curves 3). The reason is, that the value of K essentially determines the dominant mechanism of heating. When K is large, the heating mechanism is predominantly of superparamagnetic nature and generated via dynamic hysteresis, and here the interactions are seen to decrease the SAR value. At the opposite limit of low values of K, the external field amplitude is sufficient to cause hysteretic switching of particles in the system, and as a result the heating mechanism is predominantly via conventional metastable hysteresis. In this case, increasing ε results in the increasing SAR when particle diameter is small while for larger particle the trend is opposite. This behaviour is consistent with previous model calculations of Verdes *et. al.*[31], who showed that the effects of interactions on the hysteretic properties are indeed dependent on the value of KV via the parameter $\alpha = KV/kT$. For small α i.e., close to superparamagnetic systems, the interactions tend to be pairwise, leading to an enhancement of the energy barrier, whereas for hysteretic systems (large α) the microstructure is dominated by a tendency to flux closure leading to energy barrier reduction.

Fig. 5 demonstrates the important effect of interactions, via the dependence of the maximum SAR value and the optimal particle size as a function of the packing fraction ε. Consistently with Fig. 4, the interaction strength scales with ζ, and the peak value of SAR clearly decreases with increasing interaction. The decrease of the interaction effects for the larger K values is also consistent with this scaling. Clearly, the effect of interactions on the SAR, and also on the optimal particle diameter, should not be neglected. We note that these calculations are carried out for relatively low particle densities: for systems containing aggregated particles, where the local density can be significantly higher, interaction effects may be even more pronounced[7,19,21].

Discussion

We have developed a kinetic Monte-Carlo model of the underlying heating mechanisms associated with the hyperthermia phenomenon used in cancer therapy. Our work shows that the apparently different (superparamagnetic and hysteretic) mechanisms of magnetic heating have a common, hysteretic, physical origin. The so-called superparamagnetic regime is characterised by a dynamic hysteresis which transforms gradually to more conventional hysteresis arising from thermally activated transitions between metastable states. The kMC model described here captures the physics of both heating mechanisms. In the linear response regime, the kMC results are in agreement with the theory of Rosensweig[13]. Beyond this limit the nonlinear

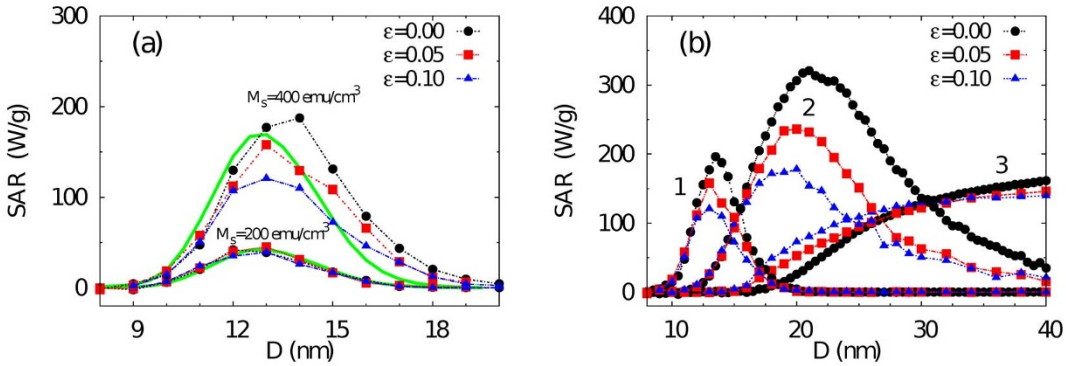

Figure 4 | SAR as a function of the mean particle size *D* for variable volumetric packing fraction ε including noninteracting case ($\varepsilon = 0$) and two values M_s = 200 emu/cm³ and 400 emu/cm³. For low M_s = 200 emu/cm³ the dipolar interactions are weak and SAR does not depend on ε. The solid line represents the solutions by means of RT. (b): SAR vs. *D* for different packing fractions and the values of $K = 3 \times 10^5$ erg/cm³ (curve set 1), 1.5×10^5 erg/cm³ (curve set 2) and 0.5×10^5 erg/cm³ (curves set 3). Calculations correspond to log-normal distributions of size and anisotropy constants both with standard deviations 0.1, spherically distributed anisotropy axes, and field amplitude H_0 = 300 Oe.

contributions, included in the kMC approach, give rise to increasing divergence from the predictions of Ref. 13, leading to significantly different SAR values and to different materials parameters for optimal heating (Fig. 6). The transition regime is characterises by two main features: 1) large values of SAR and 2) SAR dependence on D presents broad peaks. Both characteristics are ideal for hyperthermia application, therefore making the transition region of high importance.

We also carried out an investigation of the effect of dipolar interactions. The effects of interactions were found to be significant and also generally consistent with a scaling of the relative interaction strength with ζ (Fig. 5). However, the effects of interactions are also dependent on the ratio KV/k_BT since the interactions affect the properties of superparamagnetic and hysteretic systems differently as reported in Ref. 31. Interactions are rarely considered in relation to models of hyperthermia, but the results presented here suggest that their inclusion, along with detailed models of the nanoparticle structures, are extremely important for realistic predictions of the heat generation which is central to the phenomenon.

Both the non-linear behaviour induced at higher applied field amplitudes H_0 and the dipolar interactions produce a significant deviation from the RT. Figure 6 illustrates the complexity of the hyperthermia problem. The variation of the optimum SAR value as function of K is not monotonic. In the transition regime the optimum SAR value increases with decreasing K. Afterwards, when entering in the fully hysteretic regime, SAR decreases with decreasing K. In this regime, SAR vs D does not present a peak, but asymptotically reaches a saturation value with increasing size. In this case after a certain size there is no significant variation in SAR. This is shown in Fig. 6b. Considering now the interacting case, the transition towards the fully hysteric regime is not as clear as in the non-interacting case. Although the maximum SAR decreases with decreasing K, the particle size for reaching the maximum SAR is varying.

In conclusion, the kMC approach gives a unified treatment of the apparently disparate mechanisms of heating in the superparamagnetic and fully hysteretic regimes and the transition between them and, with its accurate timescale quantification, gives a reliable prediction of the frequency and particle size dependent behaviour. The inclusion of interparticle interactions leads to important and complex effects on the hysteresis which will be amplified in systems involving aggregated particles. Further development and long-term optimisation of the hyperthermia phenomenon must be cognisant of these factors and the modelling approach described here is a powerful tool for future materials and therapy design.

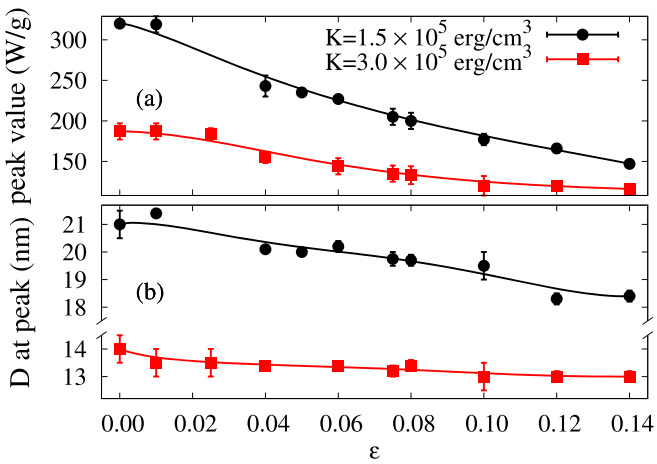

Figure 5 | Maximum SAR value (a) and peak position (b) as function packing fraction, ε for two values of anisotropy: 3×10^5 *erg/cm*³ (red squares) and 1.5×10^5 *erg/cm*³ (black circles). The lines are to guide the eye.

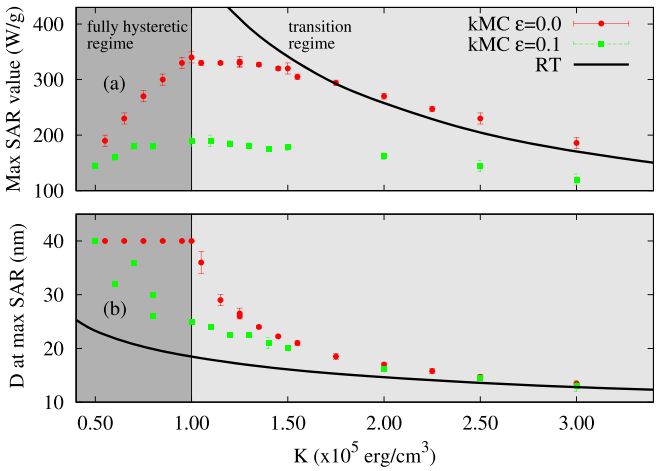

Figure 6 | Maximum SAR value (a) and the corresponding particle size (b) as function of anisotropy for: RT (black line), kMC non-interacting case (red circles) and kMC with interaction (green squares). In the fully hysteretic regime the SAR dependence on D does not present a peak, but is reaching a saturation value with increasing D.

Methods

kMC model. The basic model, which follows Ref. 26, is a collection of N Stoner-Wohlfarth spherical particles i with uniaxial anisotropy $\vec{k}_i$ and diameter D_i confined in sample volume V_s. The interaction field coupling any pair of particles i and j reads:

$$\vec{H}_i^{\mathrm{dip}} = \sum_{i \neq j} V_j M_s r_{ij}^{-3} \left(-\hat{m}_j + 3\hat{r}_{ij} \left(\hat{m}_j \cdot \hat{r}_{ij} \right) \right) \tag{4}$$

Where $\vec{r}_{ij} = r_{ij}\hat{r}_{ij}$ is the inter-particle distance. The volumetric packing fraction of particles is $\varepsilon = N\langle V_i \rangle / V_s = NV/V_s$ and the average interparticle distance is $l = (V_s/N)^{1/3}$. The system is characterised by the dipole energy ($\sim M_s^2 V^2 / l^3$), anisotropy energy (KV) and thermal energy (kT). The effect of interactions will depend on the thermal stability ($\alpha = KV/kT$) and the ratio between dipole energy and anisotropy energy ($\zeta = M_s^2 V^2 / \left(l^3 KV \right) = M_s^2 \varepsilon / K$).

Superparamagnetic behaviour occurs up to large energy barriers. Persistence in the superparamagnetic behaviour creates difficulties for standard MC approaches due to the unreasonably large number of MC steps that are necessary to achieve equilibrium. By considering the superparamagnetic particles with large energy barriers($>3kT$) as a two-state system, an improved computational approach can therefore be derived[26]. For effective local fields of particles $\vec{H} + \vec{H}_i^{\mathrm{dip}}$ less than a critical value there are two equilibrium particle states, '+' and '−', and the probability for a particle moment $\hat{m}_i$ to switch between these states is $P_i = 1 - \exp(-t/\tau_i)$[29]. The relaxation time constant τ_i is a reciprocal sum of the transition rates τ_i^+ and τ_i^- dependent on the energy barriers $\Delta E_i^{\pm}$ seen from the '+' and '−' states via the standard Néel-Arrhenius law[32]: $\tau_i^{\pm} = \tau_0 \exp\left(\Delta E_i^{\pm} / k_B T \right)$, where k_B is the Boltzmann constant and T the temperature. The method has a real time step due to the master-equation nature and can be applied for frequency up to 10^7 Hz. There is no low frequency limit for the method.

Generating particle spatial configuration. To obtain a system of random particles configuration having a certain packing fraction, ε, we start with a perfect simple cubic lattice with a large lattice spacing so that the particles do not overlap. Then the particles are randomly moved with a classical Metropolis Monte-Carlo approach. The move is accepted with the probability $\min(1, e^{(-\Delta E)})$. This step is repeated 50 times and then the system size and the inter-particle distance are reduced with an amount, for which there are no touching particles. The procedure is repeated until the desired packing fraction is obtained. Afterwards 500 more random moves are done for each particle. ΔE is calculated using a dimensionless repulsive energy of the form $E_i^{new,old} = \sum_{j=1, j \neq i}^{N} 1000 \cdot D_i \Big/ \left(r_{ij}^{new,old} \right)^4$.

Rosensweig theory. To compare and validate our kMC model with the Rosensweig theory (RT) we used all possible consideration for improving the original theory. For the equilibrium susceptibility χ_0 we used the equilibrium magnetization curves calculated as in Ref. 26, which incorporates the dependence on the distributions of particle size, anisotropy values, and anisotropy easy axis directions. In this case Eq. 1 becomes:

$$\mathcal{P} = \frac{1}{N} \sum_{i=1}^{N} \pi \mu_0 \chi_0 \left(\vec{k}_i, D_i \right) H_0^2 f \frac{2\pi f \tau_i(K_i, D_i)}{1 + \left(2\pi f \tau_i(K_i, D_i) \right)^2} \tag{5}$$

Eq. 5 allows to calculate the specific heat power for any system of non-interacting magnetic particles. For example for the ideal case when the easy axis is parallel with the field amplitude.

We calculate hysteresis curves numerically using the kMC model and from the expression arising from RT: $M(H(t)) = H_0(\chi' \cos(2\pi f t) + \chi'' \sin(2\pi f t))$. This represents the equation of an ellipse, with χ' and χ'' calculated from Eq. (3) using the linear response theory:

$$\chi' = \frac{\chi_0}{1 + (2\pi f \tau)^2} \tag{6}$$

$$\chi'' = \frac{\chi_0}{1 + (2\pi f \tau)^2} (2\pi f \tau) \tag{7}$$

Evaluating SAR. Denoting the hysteresis loop area as A, the specific heating power is computed in simulations directly as the product $\mathcal{P} = AfM_s V_t$, which is then compared with calculations based on Eq. (1) as described below. The quantity that characterises the efficiency of the heating is known as the specific absorption rate (SAR) or heat dissipation per unit mass: $\mathrm{SAR} = \mathcal{P}/m_t = AfM_s/\rho$; where ρ is the density of magnetic material, V_t/m_t is the total volume/mass of magnetic material. In this paper we consider $\rho = 5.2$ g/cm^3, the density of magnetite (Fe_3O_4).

1. Pankhurst, Q. A., Connolly, J., Jones, S. K. & Dobson, J. Applications of magnetic nanoparticles in biomedicine. *J. Phys. D: Appl. Phys.* **36**, R167–R181 (2003).
2. Laurent, S. *et al.* Magnetic iron oxide nanoparticles: synthesis, stabilization, vectorization, physicochemical characterizations, and biological applications. *Chem Rev.* **108** 2064–110 (2008).
3. Colombo, M. *et al.* Biological applications of magnetic nanoparticles. *Chem. Soc. Rev.* **41**, 4306–34 (2012).
4. Martinez-Boubeta, C. *et al.* Learning from nature to improve the heat generation of iron-oxide nanoparticles for magnetic hyperthermia applications. *Sci. Rep.* **3**, 1652 (2013).
5. Hergt, R., Dutz, S. & Röder, M. Effects of size distribution on hysteresis losses of magnetic nanoparticles for hyperthermia. *J. Phys.: Condens. Matter* **20**, 385214 (2008).
6. Mamiya, H. & Jeyadevan, B. Hyperthermic effects of dissipative structures of magnetic nanoparticles in large alternating magnetic fields. *Sci. Rep.* **1**, 157 (2011).
7. Branquinho, L. C. *et al.* Effect of magnetic dipolar interactions on nanoparticle heating efficiency: implications for cancer hyperthermia. *Sci. Rep.* **3**, 2887 (2013).
8. Suto, M. *et al.* Heat dissipation mechanism of magnetite nanoparticles in magnetic fluid hyperthermia. *J. Magn. Magn. Mater.* **321**, 1493–1496 (2009).
9. Verde, E. L., Landi, G. T., Gomes, J. A., Sousa, M. H. & Bakuzis, A. F. Magnetic hyperthermia investigation of cobalt ferrite nanoparticles: Comparison between experiment, linear response theory, and dynamic hysteresis simulations. *J. Appl. Phys.* **111**, 123902 (2012).
10. Mayergoyz, I. D. *Mathematical Models of Hysteresis*, (Springer, New York, 1991).
11. Cullity, B. D. & Graham, C. D. *Introduction to Magnetic Materials*, (John Wiley & Sons, Inc., New Jersey, 2008).
12. Zwanzig, R. *Nonequilibrium Statistical Mechanics*, (Oxford University Press, 2001).
13. Rosensweig, R. Heating magnetic fluid with alternating magnetic field. *J. Magn. Magn. Mater.* **252**, 370–374 (2002).
14. Vallejo-Fernandez, G. & O'Grady, K. Effect of the distribution of anisotropy constants on hysteresis losses for magnetic hyperthermia applications. *Appl. Phys. Lett.* **103**, 142417 (2013).
15. Hergt, R., Dutz, S., Müller, R. & Zeisberger, M. Magnetic particle hyperthermia: nanoparticle magnetism and materials development for cancer therapy. *J. Phys.: Condens. Matter* **18**, S2919–S2934 (2006).
16. Martinez-Boubeta, C. *et al.* Adjustable Hyperthermia Response of Self-Assembled Ferromagnetic Fe-MgO Core-Shell Nanoparticles by Tuning Dipole-Dipole Interactions. *Adv. Funct. Mater.* **22**, 3737–3744 (2012).
17. Sohn, H. & Victora, R. H. Optimization of magnetic anisotropy and applied fields for hyperthermia applications. *J. Appl. Phys.* **107**, 09B312 (2010).
18. Mehdaoui, B. *et al.* Optimal Size of Nanoparticles for Magnetic Hyperthermia: A Combined Theoretical and Experimental Study. *Adv. Funct. Mater.* **21**, 4573–4581 (2011).
19. Serantes, D. Influence of dipolar interactions on hyperthermia properties of ferromagnetic particles. *J. Appl. Phys.* **108**, 073918 (2010).
20. Reeves, D. B. & Weaver, J. B. Nonlinear simulations to optimize magnetic nanoparticle hyperthermia. *Appl. Phys. Lett.* **104**, 102403 (2014).
21. Serantes, D. *et al.* Multiplying Magnetic Hyperthermia Response by Nanoparticle Assembling. *J. Phys. Chem. C* **118**, 5927–5934 (2014).
22. Landi, G. T. Role of dipolar interaction in magnetic hyperthermia. *Phys. Rev. B* **89**, 014403 (2014).
23. Haase, C. & Nowak, U. Role of dipole-dipole interactions for hyperthermia heating of magnetic nanoparticle ensembles. *Phys. Rev. B* **85**(4), 045435 (Jan. 2012).
24. Carrey, J., Mehdaoui, B. & Respaud, M. Simple models of dynamic hystereis loop calculations of magnetic single-domain nanoparticles: Application to magnetic hyperthermia optimization. *J. Appl. Phys* **109**, 083921 (2011).
25. Tan, R. P., Carrey, J. & Respaud, M. Magnetic hyperthermia properties of nanoparticles inside lysosomes using kinetic Monte Carlo simulations: Influence of key parameters and dipolar interactions, and evidence for strong spatial variation of heating power. *Phys. Rev. B* **90**, 214421 (2014).
26. Chantrell, R., Walmsley, N., Gore, J. & Maylin, M. Calculations of the susceptibility of interacting superparamagnetic particles. *Phys. Rev. B* **63**, 024410 (2000).
27. Nowak, U., Chantrell, R. & Kennedy, E. Monte Carlo simulation with time step quantification in terms of Langevin dynamics. *Phys. Rev. Lett.* **84**, 163–166 (2000).
28. It is worthwhile pointing out that the M(H) behavior in the dynamical response theory regime resembles a hysteresis loop. However, this kind of hysteresis is of dynamical character and essentially associated with 'inertial' phase lag between M and H, and is fundamentally different from the type of hysteresis associated with metastability.
29. Hovorka, O., Barker, J., Friedman, G. & Chantrell, R. Role of geometrical symmetry in thermally activated processes in clusters of interacting dipolar moments. *Phys. Rev. B* **89**, 9 (2014).
30. Hergt, R. & Dutz, S. Magnetic particle hyperthermiabiophysical limitations of a visionary tumour therapy. *J. Magn. Magn. Mater.* **311**, 187–192 (2007).
31. Verdes, C. Ruiz-Diaz, B., Thompson, S., Chantrell, R. & Stancu, A. Computational model of the magnetic and transport properties of interacting fine particles. *Phys. Rev. B* **65**, 174417 (2002).
32. Néel, L. Théorie du traînage magnétique des ferromagnétiques en grains fins avec applications aux terres cuites. *Ann. géophys* (1949).

Acknowledgments

We are grateful to Dr J Popplewell and Dr R Rosensweig and Prof. S Majetich for helpful discussions and comments. This work made use of the facilities of N8 HPC provided and

funded by the N8 consortium and EPSRC (Grant No. EP/K000225/1) co-ordinated by the Universities of Leeds and Manchester and the EPSRC Small items of research equipment at the University of York ENERGY (Grant No. EP/K031589/1).

Author contributions

S.R. performed the calculations using kinetic Monte-Carlo simulation and Rosensweig theory. Discussion and interpretation of results were done by all authors. S.R. and O.H. wrote the core of the manuscript, all authors contributed to parts of it.

Additional information

Competing financial interests: The authors declare no competing financial interests.

How to cite this article: Ruta, S., Chantrell, R. & Hovorka, O. Unified model of hyperthermia via hysteresis heating in systems of interacting magnetic nanoparticles. *Sci. Rep.* **5**, 9090; DOI:10.1038/srep09090 (2015).

This work is licensed under a Creative Commons Attribution 4.0 International License. The images or other third party material in this article are included in the article's Creative Commons license, unless indicated otherwise in the credit line; if the material is not included under the Creative Commons license, users will need to obtain permission from the license holder in order to reproduce the material. To view a copy of this license, visit http://creativecommons.org/licenses/by/4.0/